Blast-wave–sphere interaction using a laser-produced plasma: An experiment motivated by supernova 1987A

Y. -G. Kang,[1,2,*] K. Nishihara,[1] H. Nishimura,[1] H. Takabe,[1] A. Sunahara,[1,†] T. Norimatsu,[1] K. Nagai,[1] H. Kim,[2] M. Nakatsuka,[1] H. J. Kong,[3] and N. J. Zabusky[1,4,‡]

[1]*Institute of Laser Engineering, Osaka University, 2-6 Yamada-Oka, Suita, Osaka 565-0871, Japan*

[2]*Department of Materials Science and Engineering, Kwangju Institute of Science and Technology, 1 Oryong-dong, Puk-gu, Kwangju 500-712, Korea*

[3]*Department of Physics, Korea Advanced Institute of Science and Technology, Yusong-gu, Taejon 305-701, Korea*

[4]*Department of Mechanical and Aerospace Engineering, Rutgers University, Piscataway, New Jersey 08854-8058*

(Received 23 April 2001; published 26 September 2001)

We present x-ray shadowgraphs from a high Mach number (~ 20) laboratory environment that simulate outward flowing ejecta matter from supernovae that interact with ambient cloud matter. Using a laser-plastic foil interaction, we generate a ''complex'' blast wave (a supersonic flow containing forward and reverse shock waves and a contact discontinuity between them) that interacts with a high-density (100 times ambient) sphere. The experimental results, including vorticity localization, compare favorably with two-dimensional axisymmetric hydrodynamic simulations.

DOI: 10.1103/PhysRevE.64.047402 PACS number(s): 52.35.Tc, 52.50.Jm, 52.72.+v, 47.32.Cc

A localized explosion or instantaneous energy release within a fluid produces a blast wave, an outward traveling shock wave [1–3]. Experimental observations [4] suggest that the approach to stagnation of a moving density layer interacting with a lower-density environment is similar to the slowing of ''ejecta'' material following a supernova blast wave [5]. We report here the first experiment of a ''complex'' blast-wave interacting with a heavier than ambient sphere. A laser-produced accelerated plasma layer collides with an ambient low-density foam and launches a high Mach number (~ 20) forward shock wave (F) into the foam, a reverse shock wave (R) in the accelerated plasma layer due to stagnation against the foam, and an intermediate contact discontinuity (CD) between them. This system of R/CD/F, we designate a complex blast wave. It travels until it collides with a heavy ceramic sphere embedded in the foam, where the sphere/foam density ratio is 100.

Planar shocks interacting with spheres and cylinders have been investigated experimentally [6–8] and numerically, in connection with a supernova shock passage through a gaseous cloud [9–11] and with vorticity deposition and hydrodynamic instabilities [12,13]. Several types of vortex rings have been observed and quantified downstream of a sphere [14]. A two-dimensional (2D) hydrodynamic complex blast-wave–cylinder interaction was simulated numerically [15], but such an environment has not yet been directly tested by experiment, which is the subject of the present investigation.

The experimental configuration and diagnostics are shown in Fig. 1. The target package is composed of a CH plastic foil (1 g/cm^3) and a ZrO_2 sphere (6 g/cm^3) embedded in a low density foam block made of the polyethyleneglycol dimethacrylate, (PEGDM: $C_{10}H_{14}O_4$, 0.06 g/cm^3), which has a fiber network structure with an average pore size of 2 μm [16]. Three beams of the Gekko XII laser [17] of wavelength 0.53 μm and of total intensity 2×10^{14} W/cm^2 irradiated the CH foil. The pulse shape is a quasi-Gaussian of 1 ns duration with a 300-ps rise time. Random phase plates were used to provide uniform laser irradiation [18]. For diagnostics, another identical laser beam irradiated an aluminum (Al) foil and the resulting plasma provided an x-ray source as backlighter for the hydrodynamic evolution to be observed.

We designed the experiment using the one-dimensional Lagrangian radiation hydrodynamic code ILESTA-1D [19] with laser beam characteristics described above. The simulation configuration is depicted in the upper part of Fig. 2(a), where the x axis coincides with that of the space-time diagram (below) of Lagrangian marker points (located nonuniformly at $t=0$). At left, for $t<1.5$ ns, we see large ablative effects (upstream moving lines). The laser ablation drives a shock wave in the CH foil that is ionized. After the shock wave passes through the CH foil around $t=1.5$ ns, the rear surface of the CH plasma expands to the foam. At $t\sim2.5$ ns

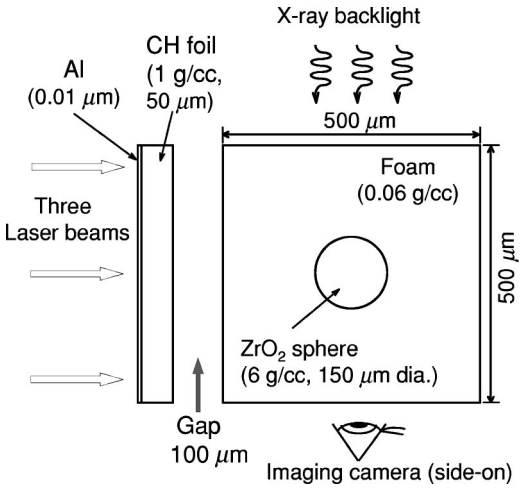

FIG. 1. Schematic view of the experimental configuration with laser drive, side-on x-ray shadowgraphy, and target package.

*Present address: Kwangju Institute of Science and Technology.

†Present address: Laboratory for Laser Energetics, University of Rochester.

‡On leave from Rutgers University.

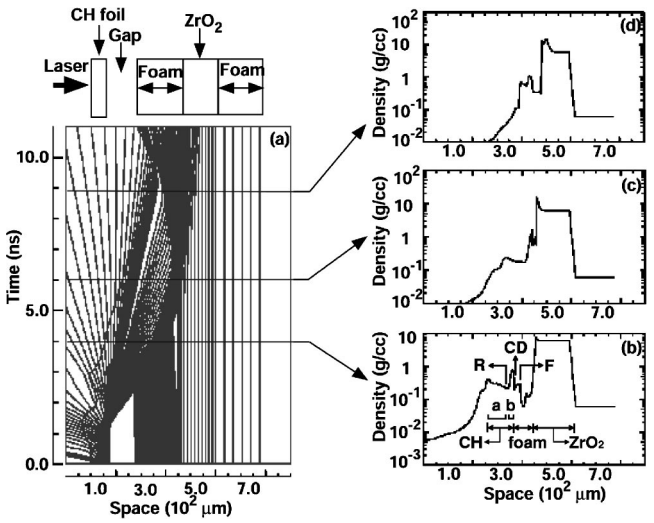

FIG. 2. Results of the hydrodynamic simulation with the code ILESTA-1D. (a) Space-time diagram of the Lagrangian marker points, nonuniformly placed at $t=0$; (b), (c), and (d) are density profiles at 4.0 ns, 6.0 ns, and 8.9 ns, respectively.

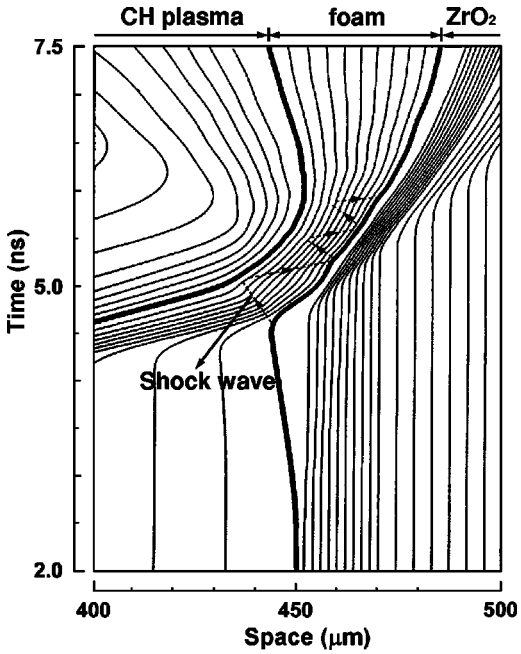

FIG. 3. Localized view of the space-time diagram of Lagrangian marker points, nonuniformly placed at $t=0$. The darker lines highlight the interfacial boundaries. Note that the incoming shock wave is reverberated.

the moving CH plasma strikes the foam and launches a forward (right) moving shock wave. The continuous CH plasma flow stagnates at a CD and a R forms in the CH plasma.

In Figs. 2(b)–2(d), we see the density at three different times, as indicated in Fig. 2(a). In Fig. 2(b), we identify three regions of different material and three discontinuities that comprise the complex blast wave. The regions are CH plasma, foam, and high-density sphere (ZrO_2). The discontinuities *R*, CD, and *F* are all moving to the right in the laboratory frame. Thus, the CH plasma consists of two regions: *a* contains the incoming CH plasma flow with a decreasing density and *b* between *R* and CD contains the stagnated CH plasma. In Fig. 2(c), CD approaches closely to the sphere and the density of the stagnated CH plasma increases further. *F* has been transmitted into the sphere and begins to compress it. In Fig. 2(d), a transmitted shock continues to propagate into the ZrO_2. Note, that a thin Al layer was deposited onto the CH foil surface (see Fig. 1) to prevent laser shine through radiation from preheating the target [20]. Nevertheless, a small-density peak near the foam-ZrO_2 interface [shown first in Fig. 2(b)] arises because energy from the radiation heat wave of the Al plasma is absorbed in this region. However, this effect is relatively weak compared to the forward shock and may be ignored.

A portion of Fig. 2(a) is amplified in Fig. 3. The slight ripples of the trajectories of incoming flows result from multiple shock reflections between the CH plasma and ZrO_2. This shock reverberation is a unique feature of the complex blast wave-sphere interaction during the early phase of evolution, and is absent in the planar shock-sphere interaction.

The x-ray transmission images or shadowgraphs are taken at various times by varying the delay time of the backlight flash with respect to that of the main drive pulse from 2 to 8.9 ns. The backlit images were recorded with an x-ray framing camera [21] with a 100-ps temporal resolution and a 30-μm spatial resolution. Figure 4 shows x-ray shadowgraphs at various times, which are approximate. This follows because each image is the result of a separate experiment where there were slight uncontrolled variations in the target package and laser conditions (including the backlighter laser). Both the shocked and unshocked foam are relatively transparent to x rays of the Al *K*-shell backlighter, while the CH plasma and the ZrO_2 sphere are more opaque. In Figs. 4(a) and 4(b), the forward shock (dotted yellow arrows) had a convex shape that arises inherently from the intensity distribution of the drive pulse on the CH foil. The laser had a focal spot with a full width at half maximum of 500 μm. In Fig. 4(c), the forward shock is not seen because it is already far downstream of the sphere. The measured velocities of the forward shock inside the foam and that of the CH plasma were $(7.0\pm1.5)\times10^6$ cm/s and $(5.0\pm1.5)\times10^6$ cm/s, respectively. The measured velocities agree well with the simulations. The observed Mach number of the forward shock was estimated to be $M=20$ from the simulations. The CH plasma (yellow arrows) close to the sphere is thicker at 6 ns than that at 8.9 ns, a phenomenon resulting possibly from the oscillating shocks in Fig. 3. As the forward shock traverses the sphere, it loses its sphericity, unlike the simulation [15], which was done with a cylinder/ambient density ratio of 5330. Figure 4(e) shows a horizontal lineout of the image at 8.9 ns and contains a triple wavy structure.

A 2D axisymmetric hydrodynamic simulation is performed for comparison with the experimental data and density results are given in Fig. 5. The code assumes an ideal, inviscid, and one temperature gas and uses a second-order Godunov scheme [22] with van Leer's flux limiter [23]. In calculating the energy transport processes, the different properties of each material are identified with the interface tracking method [24]. The simulation region corresponds to a

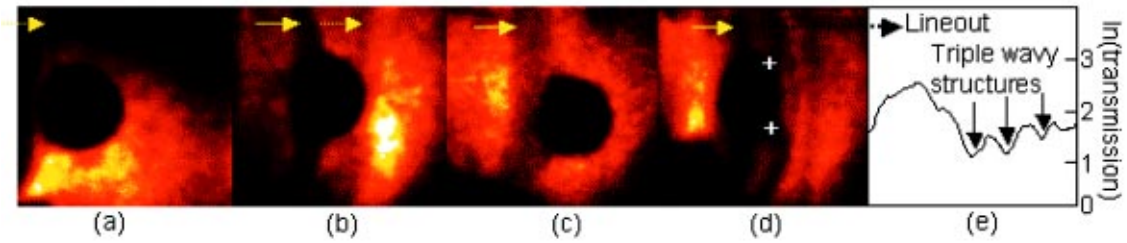

FIG. 4. (Color) X-ray shadowgraphs showing the forward shock wave (F) propagating from left to right followed by the region of CH plasma flow and interacting with the spherical target of ZrO_2. (a) $t=2.0$ ns. The forward shock, denoted by the dotted yellow arrow, is followed by the CH plasma whose upstream interface is denoted by the yellow arrow here and in the following. (b) $t=4.0$ ns. The forward shock has traversed the sphere and the curvature of the CH plasma region is evident. (c) $t=6.0$ ns. The forward shock is far downstream and not in view. The CH plasma region has become wider. (d) $t=8.9$ ns. Wavy structures are evident above and to the right of the sphere (e). Lineout of the upper region of (d), wavy structures are quantified. The y axis represents the relative intensity of the transmitted x rays in logarithm.

rectangle of 450×900 zones and includes a semicircle. The initial conditions are obtained from the 1D simulation results.

In Fig. 5(a), we see the forward shock touching the sphere, followed by the contact discontinuity and the reverse shock. In Fig. 5(b), we see the near-axis CH plasma bulging and compressed (green) and stagnated by the reverse shock as well as the interaction with the sphere. Also, the CH plasma region away from the sphere is wider than that in Fig. 5(a). In Fig. 5(c), two yellow-red regions are embedded in the green CH plasma domain, which may be due to multiple shock compression and may correspond to the wavy structures in Fig. 4(d). The well-known rollup and separation of the primary deposited vorticity [9,14] on the downstream side of a heavier than ambient sphere is evident in Fig. 5(c) and 5(d) as the ''curl'' in the CH plasma above and just downstream of the sphere. They are not clearly seen in the x-ray image, because the x-ray shadowgraphs are not sensitive to small density variations. However, we associate the white ''+'' marks of Fig. 4(d) with these curls. This conjecture is made on the basis of the curved black-red transitions in the x-ray shadowgraphs that terminates at the ''+'' marks, which are consistent with the similarly (gradually) curved CH plasma layer region in Fig. 5(c).

As the CH ejecta layer wraps around the sphere, an *oppositely signed* vortex layer may arise. This is associated with the reverberating waves within the decelerating plasma layer that is in contact with the heavier sphere. This multiple *reacceleration* environment at the front of the sphere can produce vortex double layers and strong instability and mixing effects at later times [15,25]. These issues are beyond the scope of the present paper and deserve further exploration.

In the numerical simulations, we treated the foam as a uniform gas with a low mass density of 0.06 g/cm^3. However, since the interaction of shock waves with low-density porous materials may be important to describe precisely the hydrodynamics, it is probably necessary to represent its proper equation of state [26].

We investigated an early phase of a laser produced complex blast wave-sphere interaction with an experiment and a comparable numerical simulation. The basic properties of the formation of a complex blast wave and its interaction with a heavy sphere are illustrated and salient features including the shock reverberation are exhibited. The overall qualitative hydrodynamic trends, including vorticity localization, between the experiments and the 2D simulation are similar. Future-higher spatial resolution experiments consisting of higher

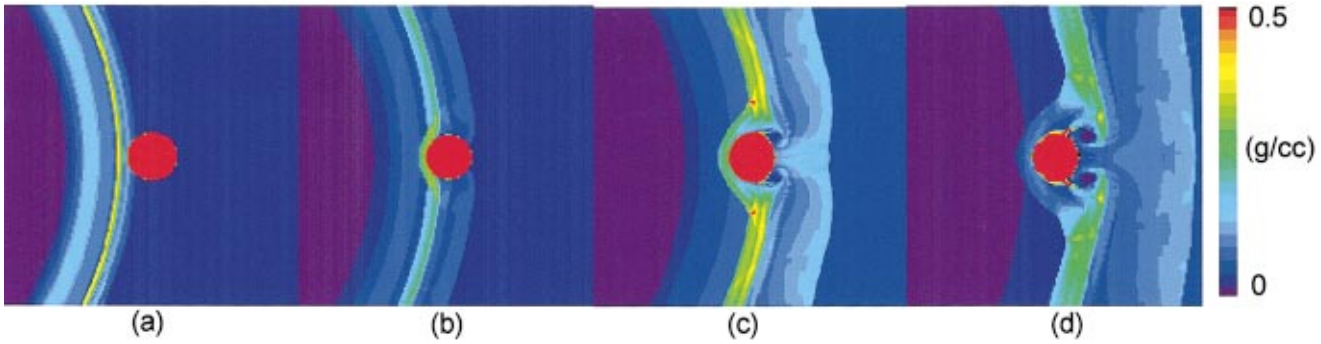

FIG. 5. (Color) Density evolution for the 2D axisymmetric hydrodynamic simulation. (a) $t=4.0$ ns. The forward shock has already begun to interact with the sphere and is followed by the upstream CH plasma. (b) $t=6.0$ ns. Forward shock at the downstream side of the sphere and bent CH plasma is in contact with the sphere. (c) $t=8.9$ ns. Forward shock downstream of the sphere generates a near-axis vortex ring and CH plasma is beginning to separate from the downstream side of the sphere. (d) $t=12.5$ ns. Separation and rollup of downstream CH plasma material close to the sphere.

precision target package and increased sensitivity due to a higher-photon energy backlighter, should clarify the precise location of shocks, vorticity localizations, and material mix. Future numerical investigations may be focused on the vortex paradigm approach [27]. This will allow us to understand the effect of nearby oppositely signed vortex double layers on the evolution of coherent structures and mixing that arises from different initial state parameters during various time epochs [28].

We acknowledge fruitful communications with S. Bulanov, N. Bobrova, S. Blinnikov, P. Lundqvist, H. Azechi, R. Kodama, D. Ryutov, B. Remington, R. P. Drake, C. F. McKee, D. Arnett, J. Kane, R. Klein, and M. Tosa, technical support of the experiments by the Gekko XII laser operation, target fabrication, and diagnostic teams. Y.-G.K. gratefully acknowledges the Hiroshi Kondo scholarship of Osaka University and support by the Korean Ministry of Education through the Brain Korea (BK21) Project.

[1] Ya.B. Zeldovich and Yu.P. Raizer, *Physics of Shock Waves and High-Temperature Hydrodynamic Phenomena* (Academic Press, New York, 1966).
[2] J. Ostriker and C.F. McKee, Rev. Mod. Phys. **60**, 1 (1988).
[3] G.S. Bisnovatyi-Kogan and S.A. Silich, Rev. Mod. Phys. **67**, 661 (1995).
[4] R.P. Drake *et al.*, Phys. Rev. Lett. **81**, 2068 (1998); R.P. Drake *et al.*, Astrophys. J. **500**, L157 (1998).
[5] R. Chevalier, Astrophys. J. **258**, 790 (1982).
[6] G. Rudinger and L.M. Sommers, J. Fluid Mech. **7**, 161 (1960).
[7] J-F. Hass and B. Sturtevant, J. Fluid Mech. **181**, 41 (1987).
[8] R. Klein, K. Budil, T. Perry, and D. Bach, Astrophys. J., Suppl. **127**, 379 (2000).
[9] K.-H. Winkler, J.W. Chalmers, S.W. Hodson, P.R. Woodward, and N.J. Zabusky, Phys. Today **40**, 28 (1987).
[10] J. Stone and M.L. Norman, Astrophys. J. **390**, L17 (1992).
[11] R. Klein, C.F. McKee, and P. Collela, Astrophys. J. **420**, 213 (1994).
[12] R. Samtaney and N.J. Zabusky, J. Fluid Mech. **269**, 45-78 (1993).
[13] J. Ray, R. Samtaney, and N.J. Zabusky, Phys. Fluids **12**, 707 (2000).
[14] N.J. Zabusky and S. Zeng, J. Fluid Mech. **362**, 327 (1998).
[15] K. Borkowski, J. Blondin, and R. McCray, Astrophys. J. **477**, 281 (1997).
[16] M. Takagi *et al.*, in *Hollow and Solid Spheres and Microspheres—Science and Technology Associated with Their Fabrication and Application*, edited by M. Berg *et al.*, MRS Symposia Proceedings No. 372 (Materals Research Society, Pittsburgh, 1995).
[17] C. Yamanaka *et al.*, IEEE J. Quantum Electron. **QE-17**, 1639 (1981).
[18] Y. Kato *et al.*, Phys. Rev. Lett. **53**, 1057 (1984).
[19] H. Takabe and T. Ishii, Jpn. J. Appl. Phys., Part 1 **32**, 5575 (1993).
[20] D.K. Bradley *et al.*, *Laser Interaction and Related Plasma Phenomena* (Plenum Press, New York, 1991), Vol. 9, p. 323.
[21] M. Katayama *et al.*, Rev. Sci. Instrum. **62**, 124 (1991).
[22] P. Colella and H.M. Glaz, J. Comput. Phys. **59**, 264 (1985).
[23] B. Van Leer, J. Comput. Phys. **32**, 101 (1979).
[24] P. Loetstedt, J. Comput. Phys. **47**, 211 (1982).
[25] H. Sakagami and K. Nishihara, Phys. Rev. Lett. **65**, 432 (1990); Phys. Fluids B **2**, 2715 (1990).
[26] M. Koenig *et al.*, Phys. Plasmas **6**, 3296 (1999).
[27] J. Hawley and N.J. Zabusky, Phys. Rev. Lett. **63**, 1241 (1989).
[28] N.J. Zabusky, Annu. Rev. Fluid Mech. **31**, 495 (1999).